literature overview of three species food chain could be nice to recycle
they do a more precise orbit description I think focusing on periodicity of limit cycles -> classifying asympt
+ a method of choosing a poincaré section

A study of a three species food chain

M.C. Varriale [a,1], A.A. Gomes [b,*]

[a] *Instituto de Matemática, UFRGS, RS, CEP 91509-900, Brazil*
[b] *CBPF, R. Xavier Sigaud 150, RJ, CEP 22290-180, Brazil*

Abstract

We study the dynamics of a food web consisting of three species of fish, extending previously obtained results. We have used two different approaches: looking for the asymptotic states of the system, resulting from numerical integration of the equations; and the application of the embedding procedure, to extract the relevant dynamical exponents, from a time series for only one scalar variable. The two approaches are complementary, the first helps emphasize geometrical aspects. In the second, orbit stability is exhibited and, via the possibility of the method of Ott et al. (Phys. Rev. Lett. 64 (1990) 1196) for chaos control, this opens issues to be studied in the future. © 1998 Elsevier Science B.V. All rights reserved.

Keywords: Attractor; Chaos; Embedding; Fish; Food chain; Limit cycles; Michaelis–Menten–Monod; Nonlinear system; Poincaré sections; Polyculture in reservoirs; Predation

1. Introduction

A large series of experimental studies involving fish have been performed; some examples are quoted in (Major, 1983; Payne and Harvey, 1989; Kirkwood et al., 1994; Patterson and Kirkwood, 1995; Persson et al., 1996). In the experimental studies, statistical methods were used to analyze the observed data. In other cases, however, some

modeling is performed together with experiments in order to compare their results; also, some management procedures are suggested. We can cite, for example, the control of warm water polyculture using native *Tucunare* with *Tilapia* (Fischer and Grant, 1994); another example is provided by the study of the effect of three predators on three preys in the presence of pollution by chemical products (Jackson, 1996). In what concerns theory, the existence of limit cycles, in predator–prey communities, was first suggested by May (1972), emphasizing the importance of nonlinear features in the models for predator–prey interactions. Pre-

* Corresponding author.
[1] Tel.: + 55 51 3366196; fax: + 55 51 3191512; e-mail: cris@mat.ufrgs.br

liminary studies, (Rosenzweig, 1973; Wollkind, 1976), have focused the importance of a three species food chain: in fact, for a continuous model, a large spectrum of complex behaviors may occur for systems with three or more species; this contrasts with the case of one or two species described by difference equations (Murray, 1993) with discrete time, implying also a complex behavior. In the above papers, however, the complete nonlinearities involved in the global behavior of the system were not fully taken into account, since the investigations have been restricted to local stability studies, through the linear approximation, near the equilibrium states. Besides the number of interacting species, another important question concerns the mathematical description of the interactions. This subject has been discussed by DeAngelis et al. (1975) and McNair (1986). For the interactions among different species, we adopt the Michaelis–Menten–Monod interaction, used in many applications to aquatic systems, including phytoplankton, zooplankton and fish. Since the solution of these equations exhibits several interesting behaviors, the present model suggests experiments using polycultures in reservoirs, to experimentally observe the corresponding time series, and then to check the predicted dynamics. The first complete study of the dynamics of three species of fish was made by Hastings and Powell (1991), who found that, for different values of a key parameter, the system exhibits several types of asymptotic motion, namely stable equilibrium point, limit cycles, change in periodicity of these cycles, and chaos. A similar type of dynamical behavior has also been observed in completely distinct kinds of nonlinear deterministic systems (Swinney, 1983; Carroll and Pecora, 1991), for example in the Belousov–Zhabotinskii chemical reaction and other mechanistic model examples.

Dynamic systems may be studied using two distinct starting points: from an experimentally observed time series or starting from a given continuous time model, via the integration of the corresponding coupled differential equations. Note that experimental determination of temporal series may perhaps be most easily performed for polycultures in small lakes or reservoirs.

In an experiment, one monitors typically only one scalar variable, and using embedding techniques to reconstruction of the phase space, we hope to recover some features of the dynamic behavior of all the system, by analyzing this single scalar signal. In order to reconstruct the dynamics of the system, from an experimental signal, we use the time delay mathematical tool (Eckmann and Ruelle, 1985), which yields several signals from a single one.

Some comments about the modeling of specific cases are worthwhile. In the case of food webs, as applied to fishes, a description of the dynamics is obtained by adopting a particular (Holling, 1965; DeAngelis et al., 1975; Hastings and Powell, 1991) kind of coupled equations, which involves a corresponding set of parameters characterizing the considered system. In certain physico-chemical cases of interest, the form of the equations is based in general laws, like the case of hydrodynamics for meteorological models (Lorenz, 1963), and the interpretation of the parameters is clear, as it is also in the case of chemical reactions. This contrasts with situations of biological interest, where the interpretation and the range of the parameters require a systematic experimental investigation, the description of the habitat, the nutrient existence and the carrying capacity among others, as mentioned in the experimental papers above.

Given the system of coupled differential equations modeling the time evolution of the system, we can choose one component $x(n)$ of its discrete time solution. This discrete time in the coupled differential equations, arises from the numerical solution method, in contrast with simpler situations like the Volterra–Lotka case (Murray, 1993) of two species, where an analytical solution does exists. This 'simulates' a measured time series. This simulation has the advantage of obtaining a larger number of points with respect to the usual experimentally obtained ones.

2. Formulation of the problem

We study in a continuous time model, the dynamic behavior of a particular ecosystem, composed by three species of fish. The feeding rela-

tionships in this three-level food chain are such that the predations occur only upon the next lower adjacent level. We label Z, the population of the species at the highest level, that preys upon Y, which is the population of the species that preys upon the member X, of the species at the lowest level of the food chain.

Let us briefly recall the description assumed by Hastings and Powell (1991). The modeling of the system was prescribed by

$$\frac{dX}{dT} = R_0 X \left(1 - \frac{X}{K_0}\right) - C_1 F_1(X) Y$$

$$\frac{dY}{dT} = F_1(X) Y - F_2(Y) Z - D_1 Y$$

$$\frac{dZ}{dT} = C_2 F_2(Y) Z - D_2 Z \tag{1}$$

with

$$F_i(U) = \frac{A_i U}{B_i + U}, \quad i = 1, 2. \tag{2}$$

The functions $F_1(X)$ and $F_2(Y)$, which multiply Y and Z, respectively, in Eq. (1), account for the interactions between two different species. Some types of interaction forms have been discussed by DeAngelis et al. (1975) and McNair (1986); here we adopt, as in Hastings and Powell (1991), the Michaelis–Menten–Monod interaction (Eq. (2)), which 'modulates' the interaction probability of the U species, via the product by the other involved population. This saturating functional response is parameterized by the constants A_i and B_i, and we verify that B_i is the value of the prey population level when the predation rate per unit prey is half its maximum value, i.e.

$$[F_i(X)]_{X=B_1} = \frac{A_1}{2} \quad \text{and} \quad [F_2(Y)]_{Y=B_2} = \frac{A_2}{2}. \tag{3}$$

Furthermore, R_0 is the intrinsic growth rate of species X and K_0 is the carrying capacity of this species; C_1^{-1} and C_2 are the conversion rates of prey-to-predator for species Y and Z, respectively; the constants D_1 and D_2 represent the death rates for each of these species, and reflect the specific characteristics of the fish pond, like nutrient availability and oxygen.

After introducing the nondimensional population variables, scaled as follows:

$$x = \frac{X}{K_0}, \qquad y = \frac{C_1 Y}{K_0}, \qquad z = \frac{C_1 Z}{C_2 K_0}, \tag{4}$$

and a new nondimensional time variable, t, obtained from the real time, T, by:

$$t = R_0 T, \tag{5}$$

the system should be described by:

$$\frac{dx}{dt} = x(1 - x) - f_1(x) y$$

$$\frac{dy}{dt} = f_1(x) y - f_2(y) z - d_1 y$$

$$\frac{dz}{dt} = f_2(y) z - d_2 z. \tag{6}$$

The parameters d_1 and d_2 are related to the constant death rates D_1 and D_2, for species Y and Z, respectively, by

$$d_1 = \frac{D_1}{R_0}, \qquad d_2 = \frac{D_2}{R_0} \tag{7}$$

Now, we have the saturating functional response, given in terms of the renormalized quantities by

$$f_i(u) = \frac{a_i u}{1 + b_i u}, \quad i = 1, 2, \tag{8}$$

parameterized by the constants a_i and b_i, related with the original parameters, through

$$a_1 = \frac{K_0 A_1}{R_0 B_1}, \qquad b_1 = \frac{K_0}{B_1},$$

$$a_2 = \frac{C_2 K_0 A_2}{C_1 R_0 B_1}, \qquad b_2 = \frac{K_0}{C_1 B_2}. \tag{9}$$

We observe that, in Eq. (8), if $b_i u \gg 1$, the saturating form $f_i(u)$ becomes nearly constant; conversely, if $b_i u \ll 1$, it is close to linear.

Thus, instead of ten original parameters, we remain with six nondimensional parameters a_i, b_i and d_i, $i = 1, 2$, for the scaled system (Eq. (6)) with the renormalized interaction strength (Eq. (8)).

3. Data processing

Briefly, we present a general summary of the method and present the numerical techniques we have used to study the dynamics of our system. In order to analyze observed data, we can use the fact that it is possible to reconstruct (Eckmann and Ruelle, 1985) some features of the dynamics of the system, from the measurements of only one scalar variable, experimentally monitored. Since, to our best knowledge, experimental results are not available for this situation, we have theoretically constructed a time series for each value of the parameter set, by using a procedure (Wolfram, 1993) for numerically integrating Eq. (6). So, we have created an output file containing 5×10^4 values of the solution for $x(t)$. This file, which is a simulation for a single scalar signal, has been the input file for the program Contemporary Signal Processor for Windows (CSPW), which is a specific software to analyze observed time series (Abarbanel, 1996). The purpose of this software is to enable us to classify and predict the behavior of a system defined via the time series, arising from a nonlinear source.

As discussed in Hastings and Powell (1991), the most important parameter in determining the dynamics for predator–prey models, like the present one, is b_1; thus, remembering the definition of this parameter, established in Eq. (9), we expect that changing the nutrient and density conditions of the fish pond, this is the most relevant parameter to change. Thus, we fixed the remaining ones, with the same values previously adopted in that reference and changed the values of b_1, in the interval from 2.0 to 4.0, following a given strategy. The choice adopted by Hastings and Powell (1991) for the parameters that were fixed, was based on their purpose to investigate biologically reasonable food chain models and to determine if chaotic dynamics were likely. Then, these authors assumed that species Y has a much larger mortality rate constant, when isolated, as compared with the isolated species Z. This implies that Z survives, when isolated, much longer than Y, in the same conditions related to biological characteristics, oxygen and absorbing capacity of the nutrients, i.e. d_1 is one order of magnitude larger than d_2. One of the ways to generate chaos is to 'periodically force' nonlinear systems that already exhibit limit cycle behavior. These authors chose parameter values that would lead to cycling in the pair of species x and y, with z absent, and also in the pair y and z, with x constant, simulating experimental situations like the absence of predator Z or a constant number of lower level X fish.

Besides the reconstruction of the phase space that we obtained from the simulation of a time series, we also looked for the asymptotic states presented by this food chain resulting from the numerical integration of Eq. (6), and eliminating the transients in the solutions; their evolution, as the b_1 parameter was increased from 2.0 to 4.0, was analyzed directly in the 3D-xyz space.

Our strategy to explore the several kinds of solutions was to divide the above defined interval in several pieces and afterwards, we refined this partition in order to better explicate the occurrence of each kind of asymptotic solution. In all these calculations, the same initial conditions were adopted.

4. The asymptotic states presented by numerical integration

Let us start with some general results extracted directly from the attractors that we obtained in the 3D-phase space for this system.

In general, we have observed that period duplication for an orbit occurs after the following procedure: firstly the resolution of the orbit decreases, which amounts to having thicker lines; also empty regions start to develop, as a preliminary step to split the orbit by shifting the no empty parts. This process is illustrated in the sequence set up in Fig. 1.

A very important point, in what concerns the obtained numerical results, is related to disregarding fluctuations associated with transient solutions; thus we extracted valid information only after 10^3 time steps. Also, in some cases we deliberately eliminate more than 10^3 time steps in order to eliminate some nontransient orbits that do not belong to the asymptotic limit, and consequently useless for our discussion.

Before the description of our results, let us now introduce the definitions and nomenclature that will be used in this work. We call a 'band' a set of
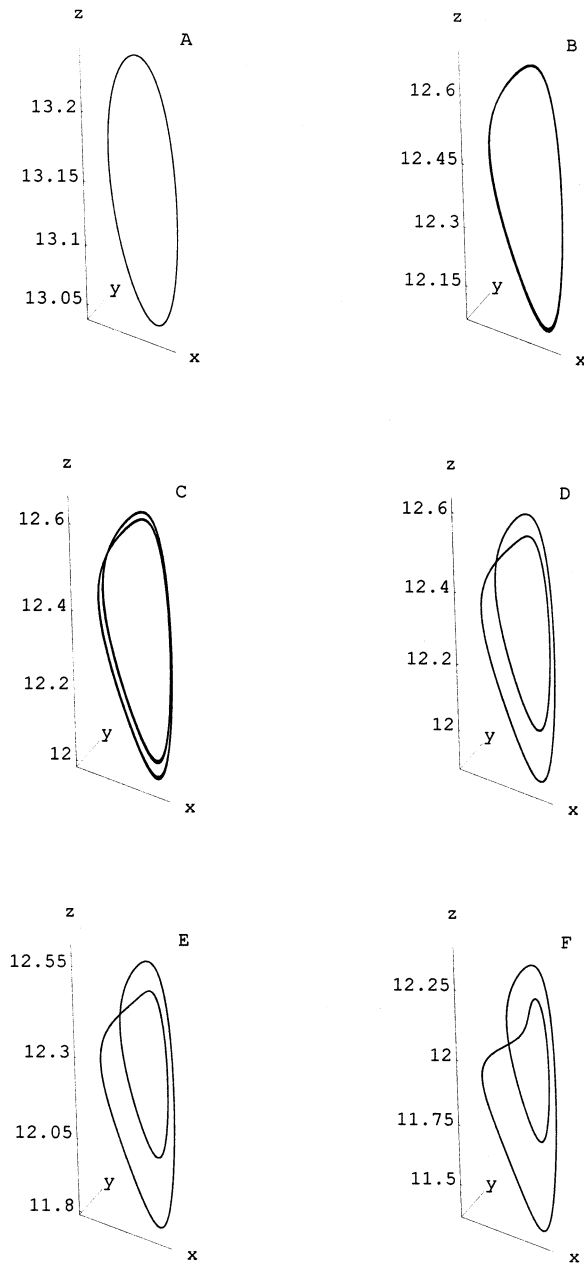
orbits very close to each other, and in certain cases some nonfilled lines may occur. In closed orbits where a period may be introduced, one may divide the cycle into open orbits: after some 'quasi-period', the system will be very close to any arbitrarily chosen starting point, to follow on the next open orbit in its trajectory.

Changing, in a systematic way, the values of the parameter b_1 we have found one of the following objects, in the asymptotic limit: the stable point, limit cycles (LC), bands (B) and a conic surface object with an upward vertex and with a handle connecting the vertex with the lower portion (S). The control parameter b_1 was increased between 2.0 and 3.2 in steps of 0.01 and, whenever necessary to make the passage from one regime to the other clearer, in steps of 0.001. More precisely, for $2.0 < b_1 < 2.39$, increments of 0.01 were enough to describe the orbits; but for greater values of b_1, we were frequently obliged to adopt smaller windows.

We have observed in these numerical experiments that the behavior of the x- and y-coordinates is different from that of the z one. Firstly, defining Δx_A, Δy_A, Δz_A as the difference between the global maximum and minimum of each component, we note that all of them increase with increasing b_1. Also, we note that whereas x- and y-components present an increase in both directions, the z-component tends to have decreasing global maxima and minima. One should note that all the orbits, namely the limit cycles, the bands, go down via the handle, thus steeply reducing the z-component from a maximum to a minimum. In the last process, the x- and y-components remain practically constant, and this fact will be of real importance for the fishery problem. After that sharp reduction, z will attain some maximum and this occurs due to the motion over the portion of the orbit lying over the conic surface. We have noted that for increasing the parameter b_1, the number of spires (turns) around the conic surface accordingly increases. The oscillations of the x- and y-components are associated to this upward motion. These oscillations are however, of a special character: while z increases, for increasing x in its oscillation, y decreases and vice versa.

Fig. 1. Duplication from the first kind of single period limit cycle, LC1s, to the second kind of double period limit cycle, LC1d; A, LC1s, $b_1 = 2.13$; B, LC1s, $b_1 = 2.28$; C, LC1d, $b_1 = 2.29$; D, LC1d, $b_1 = 2.30$; E, LC1d, $b_1 = 2.31$; F, LC1d, $b_1 = 2.37$.

For classifying the asymptotic states of our system, we present the following notation:

(a) in Fig. 7 we show the stable point (0.75, 0.13, 13.75) at $b_1 = 2.0$, which gives origin to a circular LC up to $b_1 = 2.1$;

(b) for the limit cycles we write LCn*, where $n = 1, 2, \ldots, 10$ indicates the sequence of occurrence as the parameter b_1 increases and * will be replaced by the kind of LC, namely: s (single period), d (double period), q (quadruple) or m (multiple, greater powers of 2). For example, LC3s indicates the occurence of a third kind of single period limit cycle. It should be noted that, in passing from LCns to LCnd, the formation of a new form of open orbit occurs, conserving the form of the other one;

(c) the bands are identified by Bp or BBp, etc.: recall these are formed by the set of several close orbits of the same shape; we introduced p, which assumes the values $0, 1, 2, 3, \ldots$ to specify the number of turns performed by the band around some 'axis parallel to the handle'. We will repeat the letter B to say that the band has as many parts coming from different origins. For example, we will use the notation BBB1 to indicate a band with one turn around the refered axis, in which we can distinguish basically three kinds of orbits; on the other hand, B2 will be used for just one kind of orbit, which performs two turns around this axis;

(d) to finish this description, we recall that S represents the situation where the asymptotic state is made by orbits that almost completely cover a conic surface with a handle.

We present our obtained results as a set of figures (see Figs. 2–7), each one showing some of the above mentioned asymptotic states and the corresponding values of b_1, and we will make some complementary remarks about them, as follows.

Consider the BB0 case, for $b_1 = 2.4$, one has a two-parts band, one originating in the two sets of LC1s of the last previous situation and the other from putting together the generated curves from LC1d and LC1q, already present in the last situation. These two parts coalesce for $b_1 = 2.46$, thus producing the B0 state. It should be noted that the LC3s, corresponding to $b_1 = 2.53$, was already
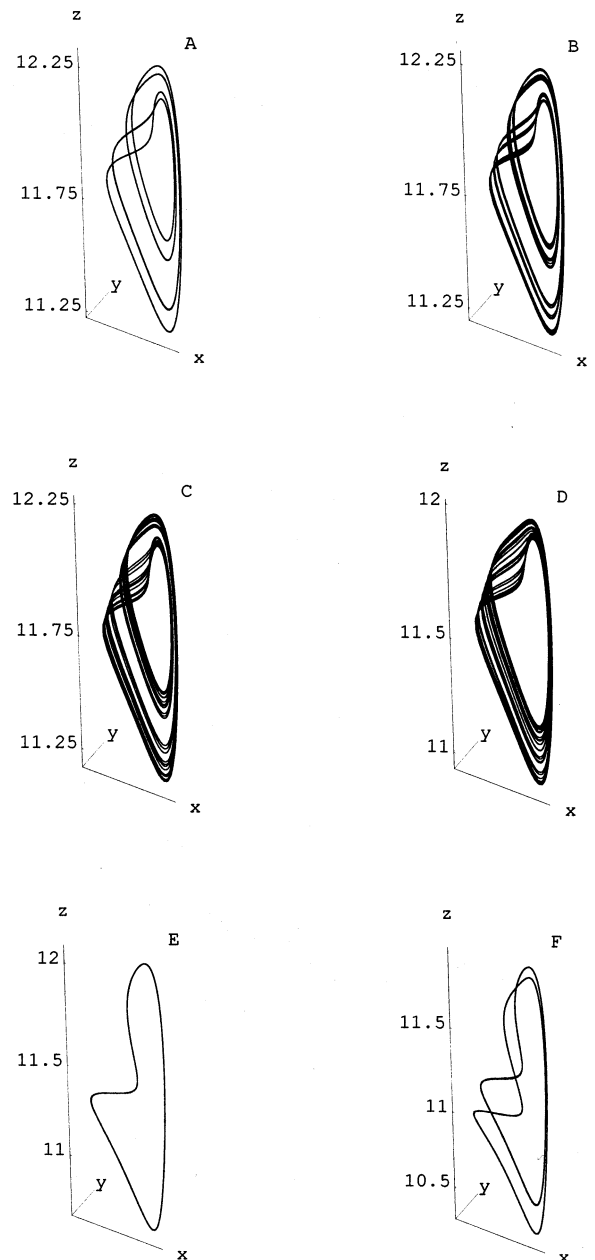

Fig. 2. Some of the asymptotic states between $b_1 = 2.39$ and $b_1 = 2.51$; A, LC1q, $b_1 = 2.39$; B, LC1m, $b_1 = 2.395$; C, BB0, $b_1 = 2.40$; D, B0, $b_1 = 2.46$; E, LC2s, $b_1 = 2.463$; F, LC2d, $b_1 = 2.51$.

present as an open orbit when generated in LC1q. The BBB1 state associated with $b_1 = 2.543$ has one part originated from LC2s, another generated

from LC1q and the last from LC1d. These three parts when grouped will compose the B1 state, for $b_1 = 2.544$. The situation for $b_1 = 2.576$ requires
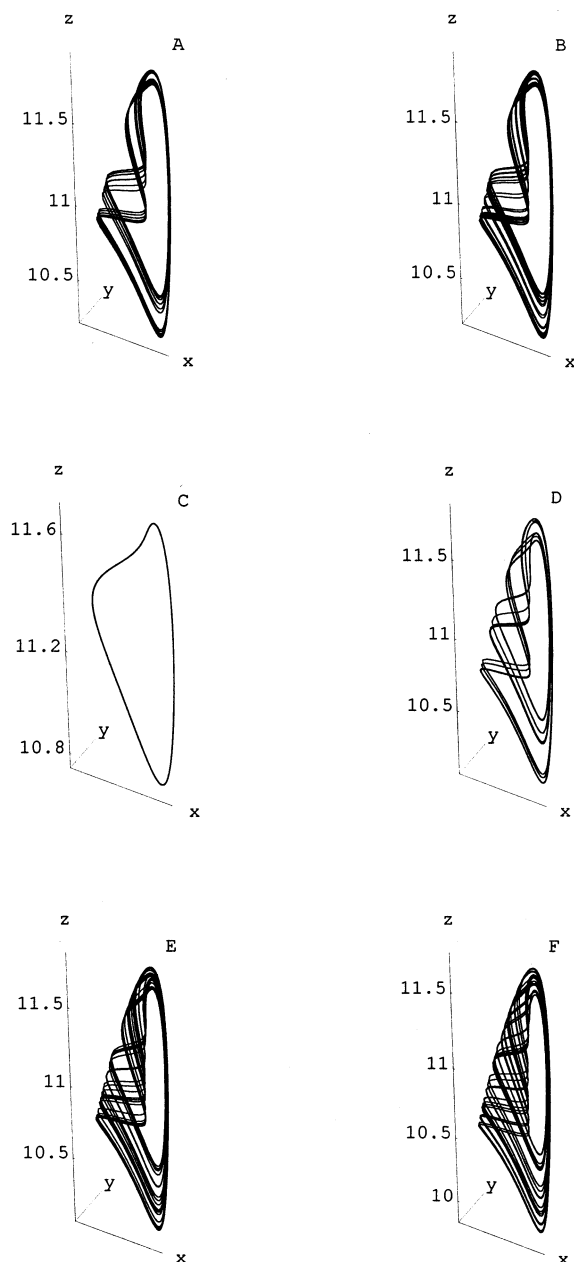

Fig. 3. Some of the asymptotic states between $b_1 = 2.52$ and $b_1 = 2.57$; A, BB1, $b_1 = 2.52$; B, BB1, $b_1 = 2.523$; C, LC3s, $b_1 = 2.53$; D, BBB1, $b_1 = 2.543$; E, B1, $b_1 = 2.544$; F, S, $b_1 = 2.57$.
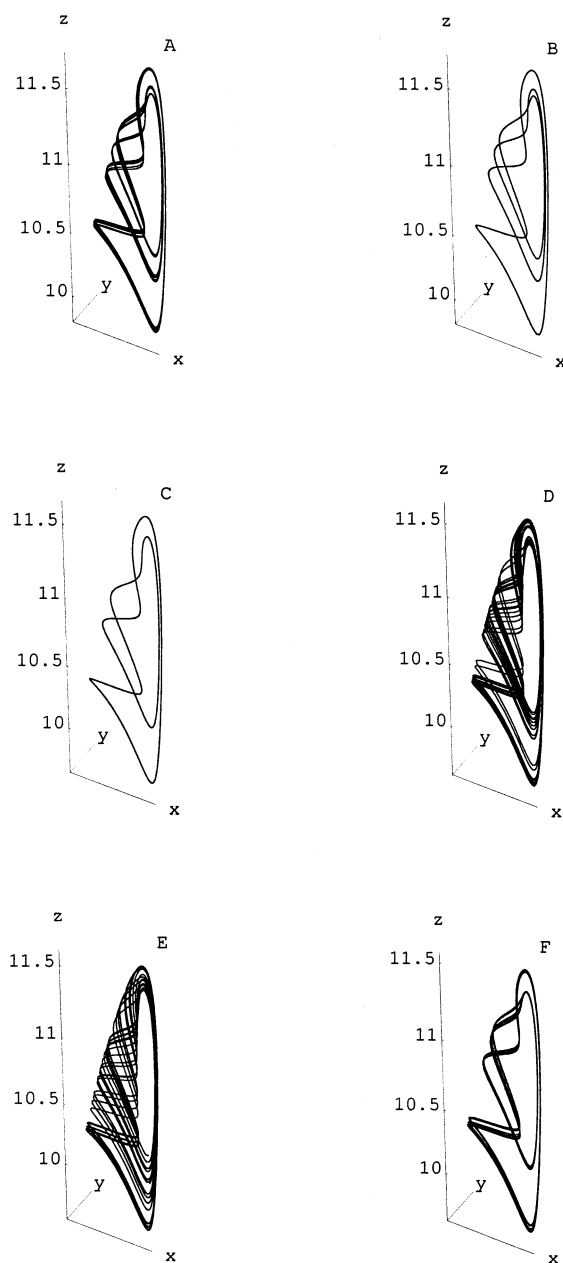

Fig. 4. Some of the asymptotic states between $b_1 = 2.576$ and $b_1 = 2.618$; A, BBB1, $b_1 = 2.576$; B, LC4s, $b_1 = 2.578$; C, LC5s, $b_1 = 2.599$; D, BBB1, $b_1 = 2.605$; E, S, $b_1 = 2.615$; F, BB1, $b_1 = 2.618$.

some explanation. The same orbits LC2s, LC1d and LC1q are involved, but the last one presents an extra turn around the conic-like surface. The

LC4s associated with $b_1 = 2.578$ exhibits the same kinds of orbits; this state is followed by the sequence LC4d, LC4m, S, and arriving at $b_1 = 2.599$
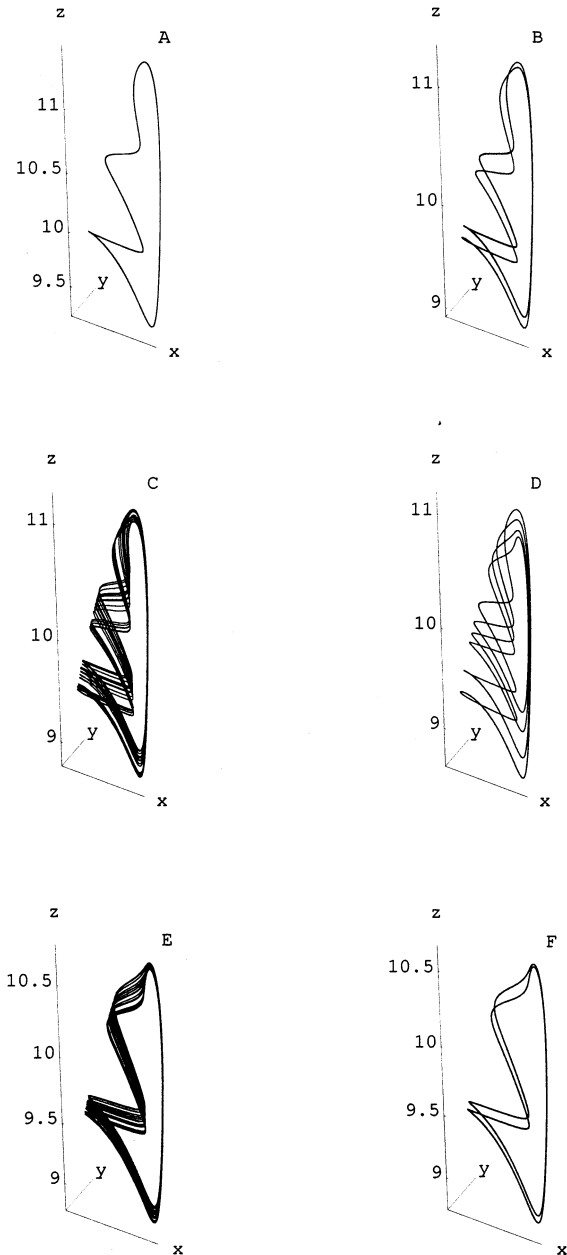

Fig. 5. Some of the asymptotic states between $b_1 = 2.661$ and $b_1 = 2.856$; A, LC6s, $b_1 = 2.661$; B, LC6d, $b_1 = 2.708$; C, B2, $b_1 = 2.735$; D, LC7s, $b_1 = 2.761$; E, B2, $b_1 = 2.832$; F, LC8d, $b_1 = 2.856$.
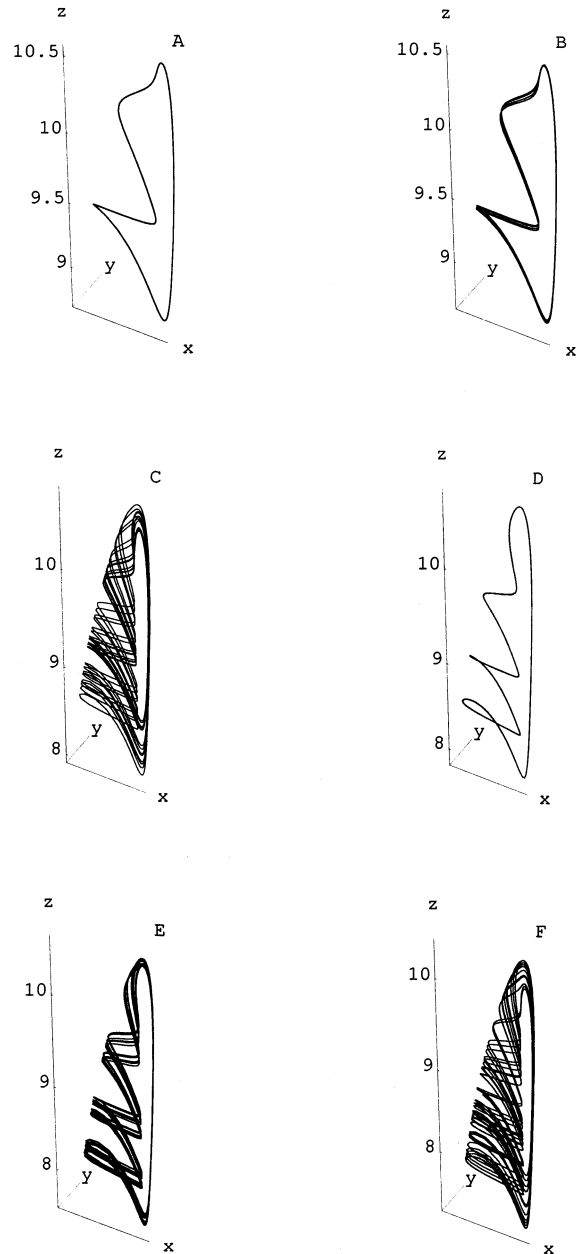

Fig. 6. Some of the asymptotic states between $b_1 = 2.879$ and $b_1 = 3.04$; A, LC8s, $b_1 = 2.879$; B, LC8m, $b_1 = 2.888$; C, S, $b_1 = 2.901$; D, LC9s, $b_1 = 2.91$; E, B3, $b_1 = 2.975$; F, S, $b_1 = 3.04$.

to stabilize the LC5s. In this cycle, only LC2s and LC1d (which now presents an extra turn) are present. By increasing b_1, after LC5d and LC5m,

one recovers for $b_1 = 2.605$, a BBB1 state, which involves the LC1q orbit, exactly as it was at 2.576. Repeating a S state once more, we remark that, for $b_1 = 2.618$, only the LC2s and LC1q (clearly with an extra turn as before) are present. After a more S state, one arrives at another limit cycle LC6s, where now the LC2s acquires an extra turn. A characteristic of the orbits originating in the single LC2s orbits, with new turns, is the following sequence: duplicate (d) originating a new form, quadruplicate (q) keeping the same forms previously existent, and after other replications finally, one observes a two-parts band BB2,
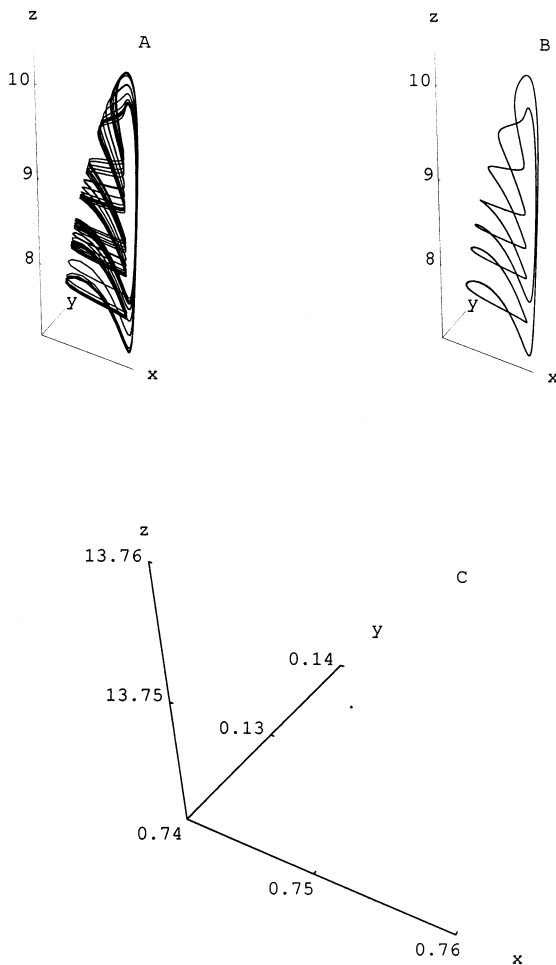

Fig. 7. The asymptotic states A, BB3, for $b_1 = 3.07$, and B, LC10s, for $b_1 = 3.076$; the stable equilibrium point at $b_1 = 2.0$ is shown in C.

to end up with a single band. This process is responsible for the occurrence of B2 at $b_1 = 2.735$. This is followed by a S state, and then the LC7s; for 2.761 in which we recognize LC6s, the one generated in LC2d, together with another identical except for an extra turn and finally, that generated in LC1q but with the extra turn already incorporated in LC4s. From these, one constructs the B2 band of 2.832, which is later followed by the LC8d, LC8s, LC8m and S states. For 2.91 we obtain the LC9s which is formed by LC6s plus another turn, followed by LC9d, LC9q, LC9m, BB3, and this finishes in a B3 at 2.975. The BB3 state corresponding to 3.07 involves simultaneously LC9s and LC8s with an extra turn. To conclude, we follow this procedure to obtain more complex limit cycles like that LC10s corresponding to $b_1 = 3.076$, with increased number of turns.

Increasing b_1 from 3.2 to 4.0 in steps of 0.1, we recovered the same kind of scenario. Besides the extraction of the typical aspects which characterize the asymptotic states of our system, we have also adopted a procedure to obtain Poincaré's sections. For each asymptotic state displayed by Mathematica Software, we can, looking to the screen of the computer, choose adequate limits for the coordinates, to select and amplify regions of the handle, where all orbits pass. We end with a cube $\Delta x = \Delta y = \Delta z$ chosen in such a way that only the handle is included within the cube. To be rigorous, with the definition of Poincaré section, one just needs to let Δz to go to very small values; however we prefered the way showed in the figures since it exhibits a small three-dimensional region. The result of this procedure for the b_1 values 2.39, 2.46, 2.52, 2.615, 2.735 and 2.901 are shown in Fig. 8. For each value, we have constructed two such sections; we observe that in some cases, by changing the scale of the interval, one passes from a completely filled band in the handle to another where the precision is enough to show empty lines. Note that we adopted scales in theses figures, such that one is the double of the other. For completeness, we have shown also the case of a LC1q in Fig. 8, which is formed only by four open orbits.
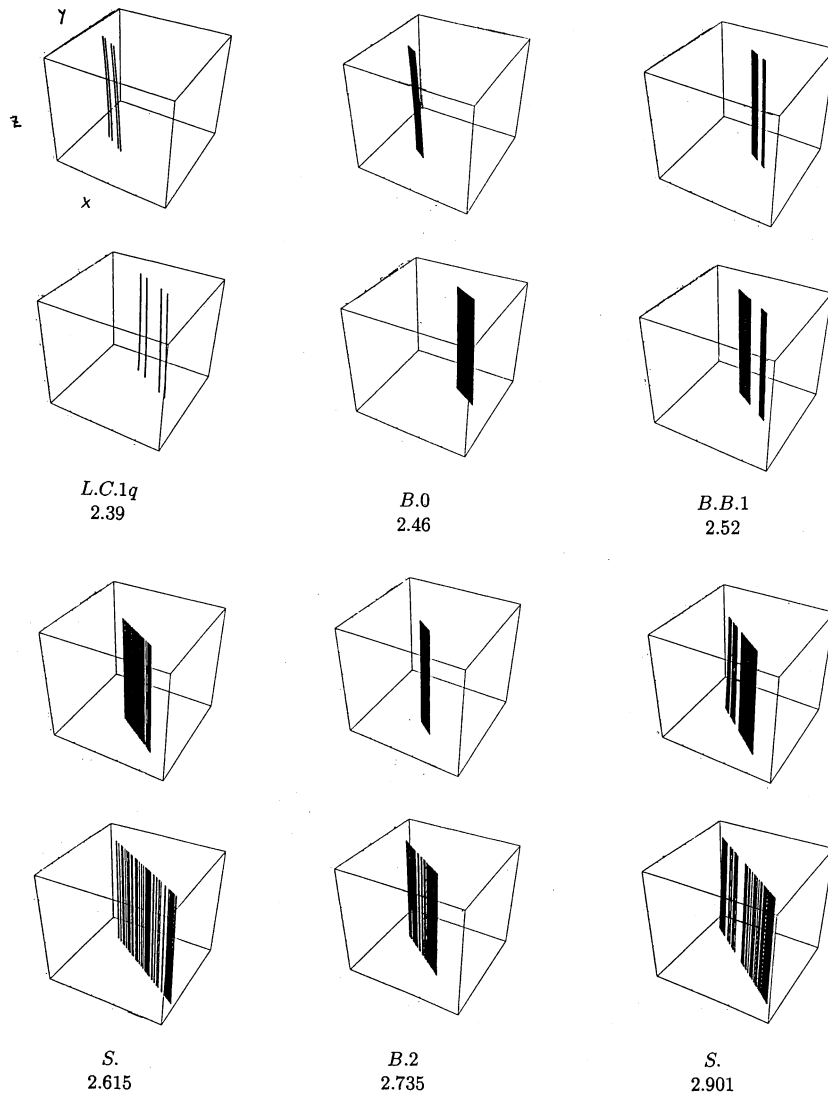
Fig. 8. Poincaré sections for $b_1 = 2.39$, 2.46, 2.52, 2.615, 2.735 and 2.901; a factor 2 in the scale distinguishes between the two sections presented for each b_1 value; the corresponding asymptotic states are also indicated, accordingly to the introduced classification.

5. The reconstructed phase space, starting from time series

As explained in Section 3, we have analyzed the dynamics of our system, through two different approaches. One of them, consisted of looking for the evolution of the asymptotic states, resulting from direct numerical integration of Eq. (6), for increments of the key parameter b_1, and this was

reported in the last section. To the second one, we have used the same procedure, to construct a time series of the single scalar variable $x(t)$, which although obtained from the numerical integration, simulates one experiment. Then, these data should be explored by the time delay mathematical tool. This procedure for reconstructing some features of all the system, from an 'experimental' signal of only one scalar variable, is available in CSPW,

which is a program containing the algorithms related with these tools.

The procedures used in CSPW to classify the dynamical objects can be briefly described as follows. The input of the CSPW program is a file of time data $s(n) = s(t_0 + n\tau_s)$, $(n = 1, \ldots, N)$, where τ_s is constant time interval between two subsequent measurements of the scalar s, which is one of the components of the system that we want to reconstruct. In our case, it corresponds to one component of the solution of Eq. (6), the x-component, and a file is associated with each given value of the parameter b_1. From CSPW, one obtains the following set of data:

(1) besides the plot of the entry data as a function of the integer n, the CSPW gives the classical quantities, namely the Fast Fourier Transform and the Linear Auto-Correlation function $C(T)$, with time lag T. The last one is defined by:

$$C(T) = \sum_n [s(n) - \bar{s}][s(n + T) - \bar{s}] \qquad (10)$$

with the average defined by $\bar{s} = \Sigma_n 1/n \, s(n)$. This quantity can be checked from experiment, using statistical routines, when an adequate experimental time series exists.

(2) the Average Mutual Information function:

$$I(T)$$

$$= \sum_{s(k)} \sum_{s(k+T)} P_{AB}(s(k), s(k+T))$$

$$\log_2 \left[\frac{P_{AB}(s(k), s(k+T))}{P_A(s(k)) \cdot P_B(s(k+T))} \right] \qquad (11)$$

where the Ps give the probabilities of single variables s, or joint probabilities, and T is a time delay, integer number of τ_s. The first minimum of this nonlinear auto-correlation function $I(T)$ provides an estimate of a time delay T_{opt}, such that variables are weakly correlated, but not so small to be disconnected; this is the time delay to use in making vectors out of the observed one-dimensional $s(k)$.

(3) the Global Dimension: d_E, is the number of dimensions necessary for unfolding our data from the axis on which it was projected, when observed, up to a full space for the dynamics; this

quantity is determined by geometric means (global false nearest neighbors for the $x(t)$ data). In the reconstructed dynamical space, d_E is an integer equal to the number of components of the vectors $[s(n), s(n + T), \ldots, s(n + (d_E - 1)T)]$.

(4) the Local Dimension: d_L, is the number of active dynamical degrees of freedom in the data; this algorithm evaluates, by dynamical predictions in dimension $d = 1, 2, \ldots, d_E$, $(d_L \leq d_E)$, the quality of predictions from models in those dimensions, and gives the percentage of bad predictions averaged over the number of starting locations for each dimension; it evaluates the predictive capability in each of the dimensions, by considering 20, 40, 60 and 80 neighbors in the model building. As the quality of prediction becomes independent of both the dimension used and the number of neighbors employed, this is the local or dynamical dimension of the dynamics; like d_E, it is an integer.

(5) the Correlation Dimension: D_2, is used to estimate a fractal dimension for the attractor, if any, associated with our data. It is one of the fractal dimensions associated with an inhomogeneous attractor; is a measure of the fractal character of the strange attractor. The algorithm estimates the average number of data points within a radius r of the data point $\vec{y}(n)$. In order to count the number of points out of the data set that are closer than radius r, or within a hypersphere of radius r, and then dividing by the total number of points, one looks at

$$C(r) = \frac{1}{MN} \sum_{k=1}^{N} \sum_{n=1}^{N} \theta(r - |\vec{y}(k) - \vec{y}(n)|) \qquad (12)$$

where M and N are typically of the order of the total number of samples. As r becomes small, the correlation dimension is defined as $C(r) \approx r^{D_2}$; so we can estimate $D_2 \cong (d \log[C(r)])/(d \log[r])$, through the slope of the curves provided by the algorithm for each value of d, $\log[C(r)] \times \log[r]$, for large enough integer-embedding dimension.

(6) the Local Lyapunov Exponents: $\lambda_a(\vec{x}, L)$, $a = 1, 2, \ldots, d_L$, determine the stability of the system and represent the growth or contraction of a perturbation to the dynamics as a function of L, where L is the number of steps along the attractor, from the perturbation. If one of them, for

large L, is positive, we have chaotic data. The sum $\lambda_1 + \lambda_2 + \ldots + \lambda d_L$ must be negative.

The stability of motions on the attractor is governed by the Lyapunov exponents, which tell how small changes in an orbit grow or shrink in time. To evaluate these, we need to estimate the local Jacobian matrices of the underlying dynamics $\vec{y}(n) \rightarrow \vec{y}(n+1)$; we have one $d_L \times d_L$ matrix at each location $\vec{y}(n)$ on the attractor. This is estimated by making a local polynomial map from neighborhood to neighborhood, and then picking off the linear term in that map. These linear terms are multiplied together L times and the eigenvalues computed for various L, and then averaged over many starting locations for perturbing the orbit. The result of this computation is the average local Lyapunov exponents $\overline{\lambda_a}(L)$; $a = 1, 2, \ldots, d_L$.

In the results presented by the algorithm, L is the number of step lengths (powers of 2) beyond the starting point and $d_{-\mathrm{Lyp}}$ is the Lyapunov dimension, which is a fractal dimension for the system. Note that when a well-defined positive exponent is detected, and using OGY techniques (Ott et al., 1990), we can stabilize a close limit cycle. This suggests experimentally to stabilize a given aquatic configuration, after the manifestation of a chaotic route.

(7) Predict: this set of algorithms allows us to construct local polynomial prediction rules on the system attractor as identified in the preceding work; from one part of the data, we learn a set of rules on how neighborhoods of points in the d_E-dimensional phase space go into other neighborhoods in temporal evolution, and, from these rules, we can interpolate in phase space to find the future evolution of new data points. On display is information about the prediction task: the actual data set, the predicted data at the same time location and the errors.

(8) CSPW software also provides a 3D graphics for the attractor, i.e. each point is defined by its first three coordinates in the d_E-dimensional reconstructed phase space; the position vector of each point is $\vec{y}(n) = [s(n), s(n + T_{\mathrm{opt}}), s(n + 2T_{\mathrm{opt}})]$.

Strictly speaking, the multi-dimensional phase portrait constructed from measurements of a single variable, by the procedure described above, gives an embedding of the original manifold.

6. Analysis of our simulated time series

We have applied CSPW to the same parameter region specified in Section 3. From the file of 50 000 points generated by numerical integration, we have used only 17 500, after eliminating the transients. Now we will present some general comments about the results of the CSPW approach.

Firstly, we verified that for all the values of b_1, CSPW-generated attractors are consistent with those that we have previously derived from numerical integration. To illustrate this we present, in Fig. 9, the reconstructed attractors for $b_1 = 2.39 \Leftrightarrow \mathrm{LC1q}$, $b_1 = 2.46 \Leftrightarrow \mathrm{B0}$, $b_1 = 2.735 \Leftrightarrow \mathrm{B2}$ and $b_1 = 2.901 \Leftrightarrow \mathrm{S}$; the choice of these values is based on the fact that they represent the different kinds of asymptotic states of our system. We also observed a growth in attractor size as the value of b_1 increases.

In all the cases of LCn*, we obtained the value 2 for the global dimension d_E; on the other hand, the local dimension is not available from the software, for any LC. This can be interpreted due to the impossibility of generating false neighbors for LCs; thus the program fails to furnish this dimension. Since these data are essential to calculate the Lyapunov exponents, these are not available in this situation. However, the attractor can be constructed and plotted, showing the characteristics of a LCn* (see for example LC1q in Fig. 9).

In the other cases, namely Bp, BBp, B...Bp, or S, both dimensions d_E, d_L and the Lyapunov exponents are calculated, with one of the exponents positive and their sum negative, as expected. Trajectories in the sheet-like attractors (band or cone-like surface) separate exponentially (stretching of the strange attractor), while trajectories off of the attractor converge exponentially to it (folding of the attractor). The stretching and folding can be directly observed by analyzing the evolution of Poincaré sections (see Section 3) at successive positions along the attractor. The Lyapunov
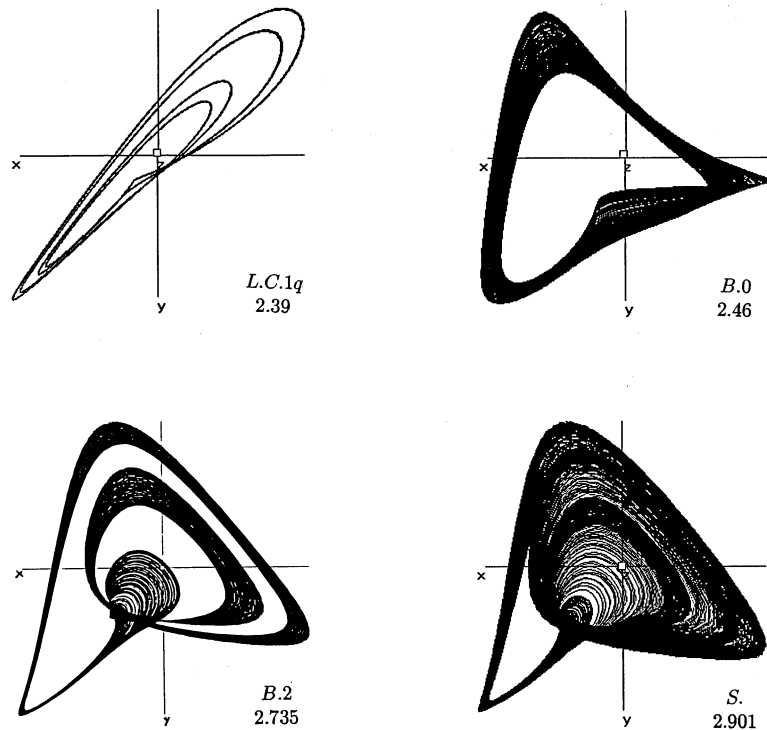
Fig. 9. Reconstructed attractors via the use of CSPW for $b_1 = 2.39$, 2.46, 2.735 and 2.901.

exponents are presented in Fig. 10, for the same values of b_1 which correspond to Fig. 9, except by $b_1 = 2.39$ because this is a LC, then, Lyapunov exponents are not available in this case. In each plot, CSPW gives us information about time delay (T_{opt}), d_E, d_L, and d_{-Lyp}. Also, we can observe by comparing the plots presented in Fig. 10, that the absolute values of the nonzero Lyapunov exponents, whenever they are available, increase with increasing values of b_1, corresponding to growth of the attractor size.

7. Conclusions

We have verified that, in this specific three species food chain, with small changes in the parameters, quite distinct behaviors are introduced, changing the types of curves/surfaces. The possibility of controlling chaos, and stabilizing a given LC could be experimentally tested in the fisheries case. This may be made by observing the changes of macroscopic parameters like carrying capacity, nutrient densities etc., and associating these with our 'microscopic' parameter, which is the responsible for the geometrical change, the others being kept fixed. This suggests that we may map the change in macroscopic behavior to the changes in one microscopic parameter.

The combination of the use of the CSPW, which is specially conceived to help experimentalists in dealing with their data, if combined and compared with the solutions of the coupled differential equations, may provide a justification for the adopted models for complex biological systems. We emphasize that this is true when a meaningful time series is available from experiment (Freeman and Kirkwood, 1995). More complex models can be systematically tested by comparing with experiment, separately changing the new ingredients of the model, e.g. using the selectivity coefficients (Jackson, 1996). Also CSPW furnishes dynamic characteristics, which are difficult to extract from the simple numerical
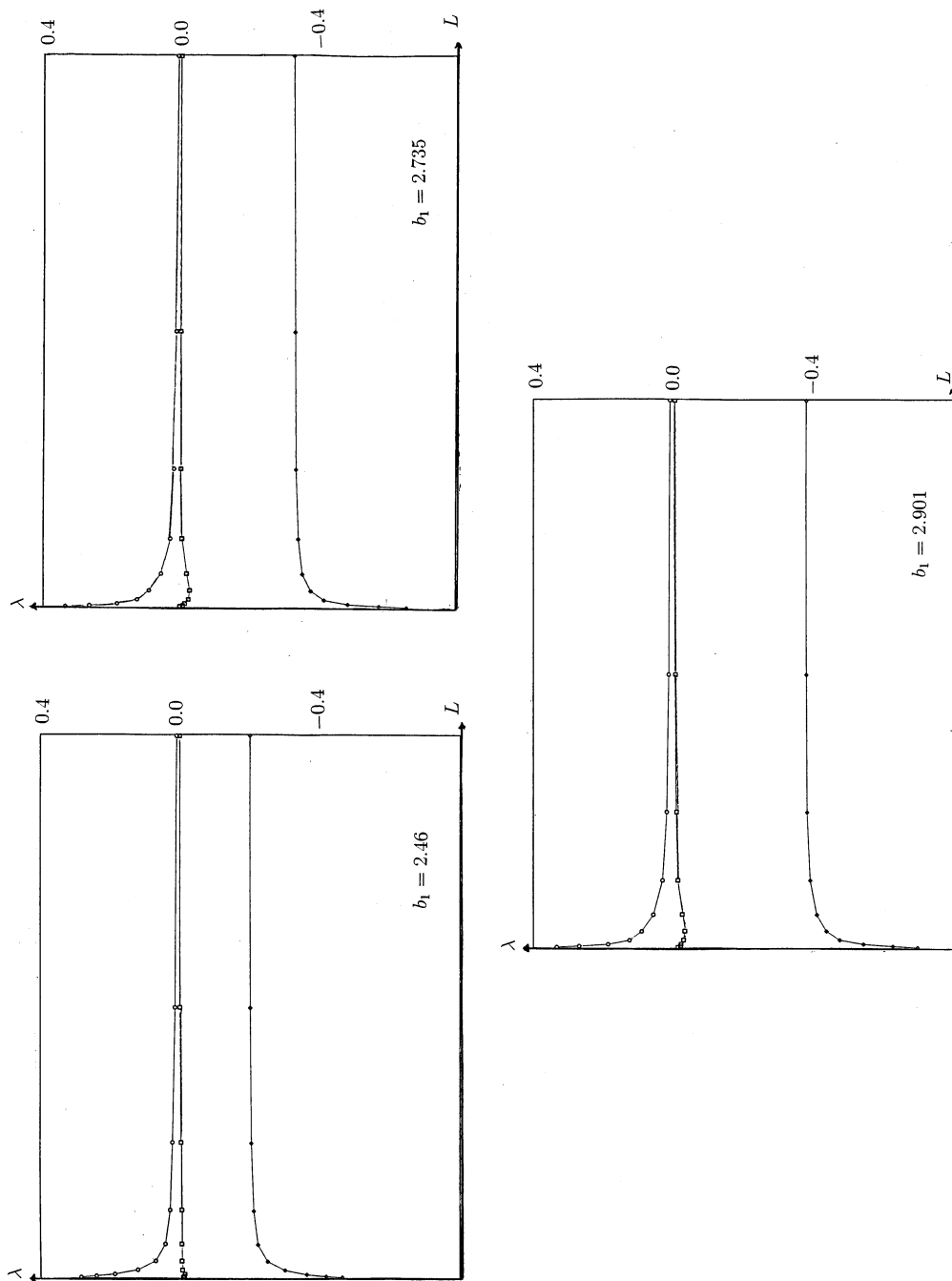
Fig. 10. The Lyapunov exponents λ vs. the number L of steps along the attractor, obtained from CSPW, for $b_1 = 2.46$, 2.735 and 2.901, for $0 \leq L \leq 2^9$. For $b_1 = 2.46$, CSPW yields $T_{opt} = 11$, $d_E = d_L = 3$ and $d_{-Lyp} = 2.028$; the values, corresponding to $b_1 = 2.735$, are $T_{opt} = 6$, $d_E = 4$, $d_L = 3$ and $d_{-Lyp} = 2.018$; for $b_1 = 2.901$, they are $T_{opt} = 6$, $d_E = d_L = 3$ and $d_{-Lyp} = 2.024$.

solutions of the differential equations defining the model. This is a large enterprise since it requires one to construct data banks during considerable time scales. However, some data banks do exist after years and the analysis, using CSPW and model constructing effort, may introduce new contributions in the understanding of these natural systems.

References

Abarbanel, H.D.I., 1996. Analysis of Observed Chaotic Data. Springer, Berlin.

Carroll, T.L., Pecora, L.M., 1991. IEEE 38, 453.

DeAngelis, D.L., Goldstein, R.A., O'Neill, 1975. Ecology 56, 881.

Eckmann, J.-P., Ruelle, D., 1985. Rev. Mod. Phys. 57, 617.

Fischer, G.W., Grant, W.E., 1994. Ecol. Model. 72, 205.

Freeman, S.N., Kirkwood, G.P., 1995. Fish. Res. 22, 77.

Hastings, A., Powell, T., 1991. Ecology 72, 896.

Holling, C.S., 1965. Mem. Ent. Soc. Can. 45, 1.

Jackson, L.J., 1996. Ecol. Model. 93, 43.

Kirkwood G.P. et al., 1994. Large-scale ecology and conservation biology, The 35th Symp. British Ecological Society with the Society for Conservation Biology, Blackwell, Oxford, reprint.

Lorenz, E.N., 1963. J. Atmos. Sci. 20, 130.

Major, P.F., 1983. Anim. Behav. 26, 760.

May, R.M., 1972. Science 177, 900.

McNair, J.N., 1986. Theor. Pop. Biol. 29, 38.

Murray, J.D., 1993. Mathematical Biology. Springer, Berlin.

Ott, E., Grebogi, C., Yorke, J.A., 1990. Phys. Rev. Lett. 64, 1196.

Patterson, K.R., Kirkwood, G.P., 1995. ICES J. Mar. Sci. 52, 183.

Payne, A.I., Harvey, M.J., 1989. Aquacult. Fish. Manag. 20, 233.

Persson, L., Andersson, J., Wahlstrom, E., 1996. Ecology 77, 900.

Rosenzweig, M.L., 1973. Am. Nat. 107, 275.

Swinney, H.L., 1983. Physica D 7, 3.

Wolfram, S., 1993. Mathematica. Addison-Wesley, Reading, MA.

Wollkind, D.J., 1976. Am. Nat. 110, 447.